# Static Light Scattering from Mixtures of Polyelectrolytes in Low Ionic Strength Solutions

**David P. Norwood, Mustapha Benmouna,† and Wayne F. Reed***

*Physics Department, Tulane University, New Orleans, Louisiana 70118*

*Received January 30, 1996*[⊗]

ABSTRACT: Static light scattering behavior is explored for salt-free and low ionic strength solutions of pure, highly charged polyelectrolytes and polyelectrolyte mixtures at very low concentration (~$10^{-5}$ g/mL). The pure polyanions (xanthan and proteoglycan subunits) show pronounced, high-contrast angular scattering peaks in the scattering function $I(q)$, whereas hyaluronate shows none. When $I(q)$ is divided by the experimentally extrapolated form factor $P(q)$ to obtain the structure function $S(q)$ using $I(q) \sim P(q)\ S(q)$, a high-contrast peak remains in $S(q)$. This can be interpreted in terms of a quasi-periodic, screened (i.e. damped) pair correlation function $g(r)$, which suggests that the peak is measuring an average interparticle separation and not any type of electrostatic scaling length. The particle/particle correlations are thought to be dynamic in the sense that no crystallization or local static ordering takes place. Adding neutral polymer (dextran) causes marked changes in $I(q)$ which can be rationalized in terms of an absence of correlation between xanthan and the polymer. Adding polyanions (hyaluronate or polystyrenesulfonate) to xanthan produces a completely different change in $I(q)$, which suggest that the xanthan molecules are being locally concentrated.

## Introduction

The static scattering properties and structures of homogeneous polyelectrolyte solutions at low ionic strength have been intensively studied for many different systems using light, X-rays, and neutrons. Comparatively little work exists, however, for the case of mixtures of polyelectrolytes. It is the object of this paper to present and interpret results for pure polyanions (proteoglycan and xanthan) and xanthan mixed with (i) simple salt, (ii) a neutral polymer (dextran), and (iii) large and small polyelectrolytes of like sign (hyaluronate and polystyrenesulfonate, respectively).

A characteristic of polyelectrolytes at concentrations far above the overlap concentration $c^*$ is the appearance of a neutron or X-ray scattering peak $I(q)$ at no added salt or very little added salt.[1−5] At concentrations on the order of 1000 times less (i.e. around 0.001% by weight), similar peaks have been observed with visible light.[6−9] At these low concentrations, generally around or below $c^*$, the peak has often been rationalized in terms of liquid-like correlations.

A brief theoretical background is given to discuss major existing models for interactions and scattering among salt-free polyelectrolyte solutions and multicomponent polyelectrolyte systems. Experimental data on the pure and mixed systems are then given, and these are partially rationalized with respect to the existing models. As will be seen, however, one needs to introduce some important modifications to these models in order to account for all of the features observed.

We do not pursue dynamic light scattering measurements in this work but point out that $1/D(q)$ ($D(q)$ is the apparent diffusion coefficient from the electric field autocorrelation decay) typically follows $I(q)$, with small deviations usually being attributed to hydrodynamic effects.[10] It is also mentioned that in this work, as well as several previous ones, there is no "slow mode" of diffusion under salt-free or low-salt conditions, as is sometimes found for some polyelectrolytes (e.g. ref 11); i.e. the presence and properties of the peak in $I(q)$ are unrelated to any diffusive slow mode for these systems. These latter, in fact, were found to be due to small populations of aggregates and/or other particles in the polyelectrolyte solutions, which could be permanently removed by proper initial filtration of the samples.[7,9,12−14]

## Theoretical Background

Several models are available in the literature which can be used to describe the scattering data from polyelectrolyte solutions. All these models have in common the fact that the charged particles interact via a long-range electrostatic potential. These have, however, specific features which depend on various properties and, in particular, on the shape of the polyions. The shape of small ions, e.g. counterions or salt ions, is usually not important. These small ions are often described as spheres with a small diameter comparable to the size of a monomer, and, in most cases, they can be viewed as point particles, especially in the analysis of the scattering data.

In general, if the contrasts of counterions and salt ions are negligible, one can write that the scattered intensity $I(q)$ is proportional to the polyion form factor $P(q)$ and the polyion−polyion structure factor $S(q)$:[15,16]

$$I(q)/KMc = P(q)\ S(q) \tag{1}$$

where $K$ is a constant which, for vertically polarized incident light, reads

$$K = 4\pi^2 n^2 (\partial n/\partial c)^2/\lambda^4 N_{av} \tag{2}$$

$n$ is the index of the refraction of the solution, $(\partial n/\partial c)$ the increment of refractive index of polymer, $\lambda$ the wavelength of the incident radiation, and $N_{av}$ Avogadro's number. The amplitude of the wave vector $q$ is related to n, $\lambda$, and $\theta$, the scattering angle, by the relationship

$$q = 4\pi n \sin(\theta/2)/\lambda \tag{3}$$

$M$ is the polyion molecular weight and $c$ its concentration.

* To whom correspondence should be addressed.
† Present address: Max-Planck-Institut für Polymerforschung, Postfach 3148 D-55021 Mainz, Germany
⊗ Abstract published in *Advance ACS Abstracts,* May 1, 1996.

S0024-9297(96)00148-9 CCC: $12.00 

The treatment of the interaction between polyions is somewhat more complicated and depends largely on their internal structure. For example, the scattering properties of charged hard spheres have been the subject of intensive investigations, both because of their relative simplicity and use in practical applications. The theories developed for simple liquids,[17] ionized gases, plasmas, metal alloys, colloidal particles,[18] etc., can be used in the case of polyelectrolyte solutions containing spherical macroions with modifications to account for their large size.

There is extensive literature on the scattering by spherical macroions.[19,20] The form factor $P(q)$ for solid spheres of diameter $\sigma$ is

$$P(q) = [3j_1(x)/x]^2 = \{3[\sin x - x \cos x]/x^3\}^2, \quad x = q\sigma/2 \quad (4)$$

The structure factor $S(q)$ for spherically symmetric objects can be written in terms of the pair correlation function $g(r) = e^{-U(r)/kT}$ as

$$S(\boldsymbol{q}) = 1 + N\int d^3\mathbf{r}[g(r) - 1]e^{i\mathbf{q}\cdot\mathbf{r}} \quad (5)$$

where $N$ is the number density of spheres, and $U(r)$ is the potential of mean force. The standard procedure is to introduce the total correlation function $h(r) = g(r) - 1$ and write the Ornstein−Zernike (OZ) equation which relates $h(r)$ to the direct correlation function $c(r)$:[17]

$$h(r) = c(r) + N\int d^3r'\, h(r - r')\, c(r') \quad (6)$$

Taking the Fourier transform of the latter equation and collecting the terms proportional to $h(q)$ yield

$$h(q) = c(q)/[1 - Nc(q)] \quad (7)$$

From eq 5 one obtains $S(q) = 1 + Nh(q)$, which is substituted into eq 7 to yield

$$S(q) = 1/[1 - Nc(q)] \quad (8)$$

Therefore, one needs to know only the Fourier transform of the direct correlation function $c(q)$ to obtain the structure factor. This requires the resolution of a set of equations comprising the OZ eq 6, together with a closure relation. The latter is usually introduced through one of the classical approximations which are well-known in the theories of liquids.[17]

Hayter and Penfold[19] applied the so-called mean spherical approximation (MSA) to charged hard spheres. In addition to the short-range hard core, this system is characterized by a long-range Debye−Hückel potential energy $U(r)$. This potential energy can be expressed in terms of the surface electric potential of the spheres $\psi_0$ as[21]

$$U(r) = \infty \quad \text{for } r < \sigma/2 \quad (9a)$$

$$U(r) = \pi\epsilon_0\epsilon\sigma^2{\psi_0}^2 e^{-\kappa(r-\sigma/2)/r} \quad \text{for } r > \sigma/2 \quad (9b)$$

where

$$\psi_0 = Z_m/[\pi\epsilon_0\epsilon\sigma(2 + \sigma\kappa)] \quad (9c)$$

$Z_m$ is the electronic charge of the macroion, $\epsilon$ is the relative dielectric permittivity, $\epsilon_0$ is the permittivity of free space, and $\kappa$ is the inverse Debye−Hückel screening length. The hard core which imposes an infinite potential to the spheres at $r = \sigma/2$ leads to the total pair correlation function $h(r)$

$$h(r) = -1 \quad \text{for } r < \sigma/2 \quad (10)$$

The MSA completes the description of the correlations between macroions in the longer range corresponding to $r > \sigma/2$ by assuming that $c(r) = -U(r)/kT$ for $r > \sigma/2$: Other closure relations give somewhat different results. In our analysis of the scattering data with polyelectrolytes with spherical shapes, we need to extend the electrostatic potential in eqs 9a,b by introducing an oscillatory damping of the interaction. This describes the data more accurately.

Another important category of polyelectrolytes which requires a different treatment are polyions having a rodlike shape. This is particularly true if the concentration and the interaction are such that a nematic order transition takes place. The most familiar example of the description of interactions between rodlike polyelectrolytes is the cylindrical cell model proposed by Katchalsky, who considered a cylindrical lattice model to solve analytically the Poisson−Boltzmann equation. The purpose of this model was to determine the variation of the electrostatic potential with the radial distance $r$. Recently, van der Maarel et al.[22,23] used a similar model to analyze a series of neutron scattering data from polyelectrolyte solutions made of DNA+TMA+-($H_2O$+$D_2O$) and PSS+TMA+($H_2O$+$D_2O$). They write the scattering intensity $I(q)$ as

$$I_{mm}(q) = \langle|\rho_m(q)|^2\rangle \quad (11)$$

where $\rho_m(q)$ is Fourier transform of the radial density of monomers. Using the cylindrical cell model, they calculate $I(q)$, assuming that the monomer density $\rho_m$-($r$) is

$$\rho_m(r) = N/\pi{r_p}^2L \quad \text{for } 0 < r < r_p \quad (12)$$

$$\rho_m(r) = 0 \quad \text{for } r > r_p \quad (13)$$

where $L$ is the contour length and $r_p$ the radius of the cylindrical lattice site. The counterion distribution was calculated by solving the Poisson−Boltzmann equation in the cylindrical geometry for which one can have an analytical solution. However, this model does not take into account the correlations between polyions and therefore describes poorly the scattering in the lower $q$ range below the scattering peak, $q_p$.

Another common example of polyelectrolytes corresponds to the intermediate situation which the chain is locally rigid but globally presents the characteristics of a flexible chain. Therefore, the treatment of the internal structure of this polyelectrolyte requires the use of the rod scheme for the local properties and a different treatment appropriate for flexible coils, with a spherical symmetry for the global properties. This was the basis of the isotropic model proposed by de Gennes et al. for semidilute polyelectrolyte solutions.

Genz et al.[10] and Grimson et al.[24] represented the long flexible polyelectrolyte as a chain of monomers or small charged spheres of diameter $d$ (pearl-necklace model) and the small ions as the monomers. The correlations between small charged spheres are evaluated by solving the MSA for the restricted primitive model. A multicomponent description formalism is used with the following partial structure factors:

$$S_{ij} = \delta_{ij} + (N_iN_j)^{1/2}h_{ij}(q) = \delta_{ij} + H_{ij}(q) \quad (14)$$

with

$$H_{ij}(q) = (N_i N_j)^{1/2} \int \mathrm{d}^3 r \; h_{ij}(r) \; \mathrm{e}^{i\mathbf{q}\cdot\mathbf{r}} \qquad (15)$$

$$h_{ij}(r) = g_{ij}(r) - 1 \qquad (16)$$

The calculation of the total correlation functions $h_{ij}(r)$ proceeds in a way similar to that in the work of Hayter and co-workers using a matrix formulation to include all of the components in the mixture.

In this work, we report and discuss static light scattering data obtained from mixtures of polyelectrolytes in aqueous solutions with and without added salt. The purpose of this investigation is to explore the effects of strong electrostatic interactions between different types of polyions on the structural properties of the mixture. Such a study is important in order to better understand the interactions between different species of polyelectrolytes prior to the formation of complexes and superstructures. To our knowledge, such mixtures have not been studied before by light scattering techniques.

The data can be analyzed using a multicomponent description, whereby the contribution of counterions to the scattering signal is reduced to screening the electrostatic interactions between polyions. In a three component system with polymer A and polymer B in a solvent, the total scattered intensity for this mixture $I(q)$ can be written as[25]

$$I(q) = I_{aa}(q) + I_{bb}(q) + 2I_{ab}(q) \qquad (17)$$

with

$$I_{ij}(q) = K(\partial n/\partial c)_i (\partial n/\partial c)_j [M_i M_j c_i c_j P_j(q) \; P_j(q)]^{1/2} S_{ij}(q) \qquad i,j = a,b \quad (18)$$

where the partial structure factors $S_{ij}(q)$ are equal to $h_{ij}(q)$.

## Experimental Section

**Light Scattering.** A Wyatt Dawn-F DSP, equipped with a vertically polarized 5 mW helium−neon laser operating at $\lambda = 632$ nm and 18 simultaneously detected scattering angles, was used. The inventor has recently described the instrument.[26] The Dawn-F is equipped with an on-board 16 bit A/D converter to digitize the 0−10 V signals from each photodiode. Serial transmission of the 18 angles was made to an IBM 80486DX-66 microcomputer every half-second via a standard RS232-c cable. W.F.R. wrote the control and data acquisition programs for the Dawn. For each instrument, typically 200 separate measurements of the scattering at each photodetector were taken, and the minimum at each was selected. This procedure eliminates spuriously high scattering signals from stray light (the sample cell is slowly rotated during the measurements) and from "dust" and other impurities. The voltage distribution about the mean is extremely narrow (standard deviations in intensity divided by average voltages are typically around 0.002) compared to the large swings from spurious scattering events, so that taking the minimum value has a virtually negligible error associated with it compared to the deleterious effect that averaging in spurious signals would have.

**Materials.** Xanthan was a gift from Systems Bioindustries (Baupte, France). Extensive literature on xanthan exists,[27−30] although no consensus exists on whether it is a single- or double-stranded polymer in solution. From static light scattering, this xanthan has $M_w \sim 3.6 \times 10^6$ and $R_g \sim 268$ nm at high ionic strength.

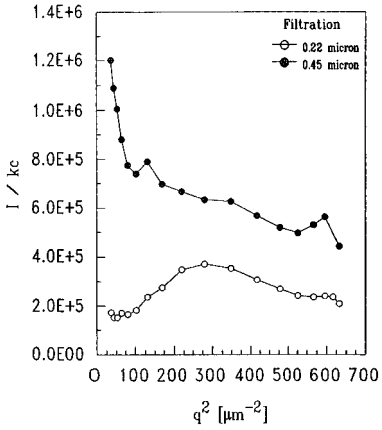


**Figure 1.** $I(q)/Kc$ for xanthan in pure water, filtered through a 0.45 $\mu$m filter (upper line) and through a 0.22 $\mu$m filter (lower line). Associated with the above line is also a slow mode of diffusion, whereas for the filtration by 0.22 $\mu$m, aggregates and other particles are removed, and the peak in $I(q)/Kc$ is visible and no slow mode of diffusion is found by dynamic light scattering.

**Table 1. Properties of the Polymers Used**

| polymer | $M_w$ (g·mol$^{-1}$) | $\xi$ | $L_0$ (Å) |
|---|---|---|---|
| dextran | $15 \times 10^3$ | 0 | 10 |
| PSS (small) | $35 \times 10^3$ | −1 | 15 |
| xanthan | $3.6 \times 10^6$ | −1 | 1250 [29] |
| HA | $1.5 \times 10^6$ | −0.7 | 90 [32] |

Hyaluronate (HA) was from Sigma Chemical Co. and was of bacterial origin (*Streptococcus zooepidemicus*). Sodium poly(styrenesulfonate) (PSS) was from Pressure Chemical Co.

Table 1 contains a summary of the weight averaged mass $M_w$, linear charge density $\xi$ (in terms of elementary charges per Bjerrum length, where the latter is about 7.2 Å in water at 25 °C), and intrinsic persistence length for the polymers used. The values of $\xi = -1$ assume the polymer is condensed to the "Manning condensation limit". $(\partial n/\partial c)$ is roughly the same for all of the polymers, being around 0.155 for HA, xanthan, and dextran and 0.189 for PSS.

The scattering behavior of the various polyanion systems was obtained by serial dilution with stock solutions of salt or different polyanion, in such a way that the original concentration of polyanion (xanthan) changed by no more than 10% during the entire dilution.

**Importance of Proper Filtration in Removing Aggregates/Other Particles and "Slow Modes" of Diffusion.** As in all of our previous investigations of polyelectrolytes at very low ionic strength, we found the membrane filter pore size of critical importance in preparing the xanthan solutions. Namely, if the salt-free solutions were filtered through membranes of pore size 0.45 $\mu$m, no peak in $I(q)$ was obtained, but rather a monotonically decreasing $I(q)$, typical of neutral polymers or polyelectrolytes with added salt. Such an $I(q)$ is shown in Figure 1 for a 0.03 mg/mL salt-free xanthan solution. Dynamic light scattering on this solution showed a "slow mode", which we have found to be characteristic of polyelectrolyte solutions which have not been properly filtered and still contain a small, residual population of undissolved aggregates and/or other particles.[7,9,12,13,31] In contrast, when the same salt-free stock solution was filtered through a membrane of 0.22 $\mu$m, a clear peak in $I(q)$ was obtained, as shown in Figure 1. Dynamic light scattering on this solution revealed no detectable slow mode, indicating, within our interpretation, that this slow mode was originally due to the aggregates/other particles responsible for the monotonic decrease in $I(q)$, which were successfully removed by filtering through the smaller pore size. Measurements with the differential refractometer indicated that the loss of xanthan mass in filtering a stock solution through a 0.22 $\mu$m membrane was between 5 and 10%. This level of small material loss is consistent with our earlier reports on the permanent removal of the slow mode for such

polyelectrolytes as poly-L-lysine,[12] PSS,[12,13] chondroitin sulfate, heparin, copolymers of polyacrylamide/polyacrylate,[31] proteoglycans,[7] and succinoglycan.[9] The fact that the slow mode never reappeared in these systems has been taken as further evidence that the slow mode represents a non-equilibrium state of the polyelectrolyte solution. Such permanent removal of the slow mode in the case of PSS has been recently corroborated by independent investigators.[14] The fact that the presence of the slow mode in xanthan is actually antagonistic toward observing the peak, i.e. for this case, the presence of the slow mode implies the absence of a peak in $I(q)$ (Figure 1), is consistent with our previous experience with proteoglycan subunits and succinoglycans. In these latter cases the peak in $I(q)$ was observed when no slow mode was present, but incomplete filtration of these same solutions led to slow modes with $I(q)$ peaks of highly diminished contrast.

## Results and Discussion

**I. Scattering from Pure Polyelectrolytes at Extremely Low Ionic Strength.** We first examine LS for salt-free and low-salt solutions of three high mass (order of $1 \times 10^6$), highly charged polyelectrolytes of different "architecture": (i) proteoglycan monomers (PG), which are quite compact and amenable to spherical symmetry (data from ref 7 is used), (ii) xanthan, which is intrinsically quite stiff and most likely resembles a wormlike chain with a significant number of Kuhn lengths, and (iii) hyaluronate (HA), which is semiflexible and coillike even at low effective salt,[32] and for which no peak is measurable within experimental resolution.

**Case of a Compact Polyelectrolyte: Proteoglycan Subunit.** Proteoglycan subunits (PGS) consist of a protein backbone to which are covalently bound many, highly charged anionic oligo- and polysaccharide (glycosaminoglycan) side groups.[33−35] The PGS are thus simply branched or "comb" polymers. The masses are typically 1−2 million, and the contour lengths of the backbone are on the order of 5000 Å. Though not literally spheroidal, the PGS adopt dense, random-coillike structures in solution, which, when dilute enough, can be taken as roughly spherical.

Figure 2a shows $I(q)$ vs $q$ for PGS (mass around 1.2 million) at a concentration of [PGS] = 0.253 mg/mL, for different ionic strengths $C_s$ (adapted from ref 7). In ref 7, $P(q)$ of the PGS at no added salt was found by extrapolation to be

$$\lim_{C_s \to 0} P(q) = \frac{1}{1 + 2.76 \sin^2(\theta/2)} \tag{19}$$

Following the procedure of ref 7, Figure 2b shows $S(q) = I(q)/KcMP(q)$. It is immediately striking that the $S(q)$ at the lowest $C_s$ retain high-contrast peaks and are not, for example, monotonically increasing functions, as predicted by "correlation hole" arguments. It is also noted that even if the $I(q)$ are divided by the $P(q)$ corresponding to full rodlike stretching of the PGS, rather than eq 19, the peaks are retained. The peak in $S(q)$ also excludes models based on the transform of a screened Coulomb potential for point charges, which gives a dependence like[25,36] $S(q) \propto q^2/(\kappa^2 + q^2)$, which has no peak.

Importantly, the high contrast of the low $C_s$ peaks in Figure 2b is too high for the particles to be interacting as effective hard spheres (where the PGS have an electrostatically enhanced effective radius). We define contrast $\varsigma$ by

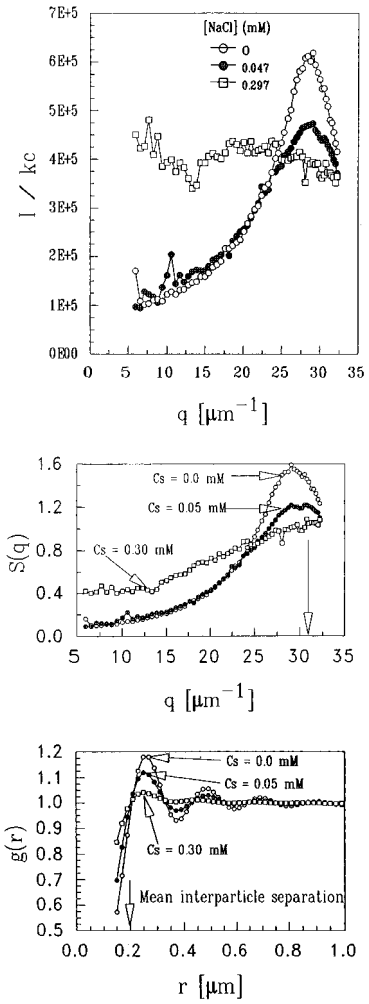


**Figure 2.** (a, top) $I(q)/Kc$ for proteoglycan subunits at different values of added salt $C_s$. (b, middle) $S(q)$ for PGS at 0.253 mg/mL, computed from eq 1 using the $I(q)$ of a and $P(q)$ of eq 19. (c, bottom) $g(r)$ for PGS computed from $S(q)$ of b. The mean interparticle separation is from $d = 2\pi/q_p$, where $q_p$ is from eq 22.

$$\varsigma = \frac{S_{peak} - S_{min}}{S_{peak} - S(q=0)} \tag{20}$$

In the case of high real or effective concentration of hard spheres, $S(q)$ is given by[37]

$$S(q) = 1 - 4\pi N R^3 \left[\frac{\sin x - x \cos x}{x^3}\right] \tag{21}$$

where $R$ is the real or effective radius of the square well, $N$ is the particle number density, and $x = qR$. There is indeed a peak in this $S(q)$, but its contrast of $\varsigma = 0.112$ is far less than that seen for either proteoglycans,[7] succinoglycan,[9] or the xanthan data, shown below. In fact, for PG at no salt (Figure 2b) the contrast is greater than 0.27 (it is greater than this because the true $S_{min}$ occurs at a value of $q$ too high to measure). In Figure 11 of ref 7, where [PG] varies from 0.12 to 0.2 mg/mL, $\varsigma$ is about 0.65. Likewise, for the xanthan data shown below (Figure 5b), $\varsigma$ varies from at least 0.22 to 0.45. The fact that a square well or similar potential is now excluded (more realistic potentials would have "softer" edges than a true square well, diminishing $\varsigma$ even further) leads us to conclude that longer range interactions, including at least second nearest neighbors, are involved, which will require some oscillatory behavior in $g(r)$, as discussed below.

As shown in refs 7 and 38, the wave vector at the scattering peak $q_p$, varies as about $c^{1/3}$, which is characteristic of a "cubic" disposition of scatterers. This is also consistent with other findings, in which at low $c$ (i.e. below the overlap concentration $c^*$) $q_p \propto c^{1/3}$, even for rodlike particles like tobacco mosaic virus[5] and DNA.[4] For such particles there is an "elbow" region around $c^*$, and at high enough concentrations $q_p \propto c^{1/2}$. For a simple cubic disposition of scatterers

$$q_p\ (\mathrm{cm}^{-1}) = 2\pi[cN_A/M]^{1/3} \qquad (22)$$

The arrow in Figure 2b shows the computed value of $q_p$ from the above formula, using $M = 1.2$ million. This value is quite close to the experimental peak, and the relatively small deviation may be due to such factors as errors in $M$, polydispersity of the particles, and a different geometrical factor which might be more appropriate than that of the simple approximation of a purely cubic disposition of scatterers. Thus, the main conclusion is that $q_p$ is measuring mean interparticle separation and not some other length scale (e.g. it does not measure an effective particle radius roughly equal to the screening length $1/\kappa$). The fact that there is no apparent shift in $q_p$ as salt is added strengthens the interpretation that $q_p$ is measuring interparticle separation and not a characteristic electrostatic screening length.

It is important to stress that the cubic disposition of scatterers leading to $q_p \propto c^{1/3}$ in no way implies any long-range order or liquid crystalline state of the polyelectrolytes in the limit of no or extremely low added salt. In fact, recent measurements of the light scattering from PGS under shear flow in size exclusion chromatography conditions[38] yielded the same types of peaks as seen in Figure 2a, also implying that the existence of the peaks is unrelated to any long-range order or structures in solution, since these would presumably be destroyed by the shear flow.

Figure 2c shows the computation, using a Parzen window (see Appendix) of the two particle distribution function $g(r)$ from the structure factor $S(q)$, adapted from eq 5 above, in the operational form

$$g(r) = 1 + \frac{1}{2\pi^2 Nr}\int q[S(q) - 1]\sin(qr)\,\mathrm{d}q \qquad (23)$$

The transform is, in principle, over all values of $q$, whereas experimental limitations force a finite (rather than continuous) sampling of $S(q)$ and also limit the range, imposing high- and low-$q$ limits. These limitations and their effect on the validity of the $g(r)$ so obtained are discussed in the Appendix, but, briefly, one is justified in using eq 23 only when the experimental error is small compared to the amplitude of the structure factor ($\mathrm{d}S \ll [S_{max} - S_{min}]$), and so long as the structure factor has a high variation ($[S_{max} - S_{min}] \sim [S_{max} + S_{min}]$).

The oscillations in $g(r)$ are striking and immediately remove the system from being conceptualized as pure, effective hard spheres. In view of the high interparticle interaction energies at low shielding, nearest neighbors are correlated strongly enough that the effect of the second nearest neighbor on the nearest neighbor must also be taken into account. A physically reasonable phenomenological model which captures this notion is that of a highly damped, quasi-periodic screened potential which yields the type of high-contrast peaks of Figure 2b. Such an interparticle potential may be constructed as

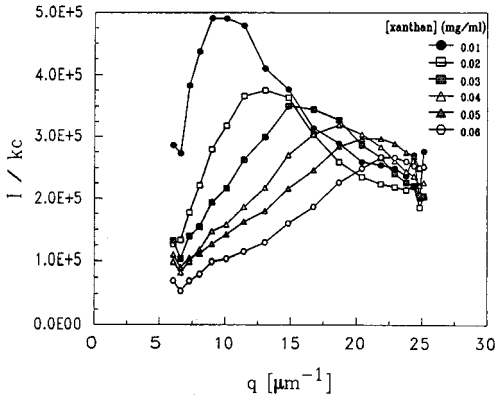


**Figure 3.** $I(q)/Kc$ for xanthan in pure water for various xanthan concentrations.

$$U(r) = U_0\frac{\cos(2\pi r/R)\mathrm{e}^{-\kappa r}}{r} \qquad r > R/2 \qquad (24)$$

Note that this form for $U(r)$ is singular as $r$ approaches 0 and is therefore not appropriate for small $r$. Being a damped force, it is quasi-periodic, with the quasi-period of $R$ ($R$ = average interparticle spacing) corresponding to minima in potential energy at multiples of the average interparticle spacing. These minima necessarily imply the involvement of at least three particles, all interacting via repulsive potentials; i.e. for two purely repulsive particles to maintain a separation near $R$, there must be a third repulsive particle at $r > R$ from the first which causes an energy penalty if the particle between it and the first moves in its direction.

As long as $U(R) > kT$, neighboring particles will preferentially occupy their energy minima near $R$, due to the above argument. As a further consequence, the peak position does not move with *small* quantities of added salt as long as this energy condition continues to hold. Equations 9b,c can be used for a very rough estimation of $U(R)$ between two PGS molecules, taken as spheres of radius $\sigma/2 = 60$ nm separated by $R = 200$ nm at [PGS] = 0.253 mg/mL for $M = 1.2 \times 10^6$, and $Z_m = 2220$ (approximate titration charge, estimated from 1 charge/540 Da of mass). This yields values of $U(R{=}200\mathrm{nm}) \sim 18200kT$ (clearly a serious overestimate) in the unscreened limit to $U(R{=}200\mathrm{nm}) \sim 0.95kT$ if the screening is assumed to be due to PGS counterions according to $\kappa = [4\pi l_B Z_m N]^{1/2} \sim 50\ \mu\mathrm{m}^{-1}$, where $N$ is the macroion particle density. Thus, it is reasonable to assume, within these limits, that there exists a strong repulsion between nearest neighbors which serves to maintain a separation of $R$ between nearby particles. While the energy could be reduced by increasing the separation between two neighbors, again this necessarily increases the interaction between neighbors on the opposite sides. A separation of $R$ represents a minimum in the repulsive energy. At a distance of $2R$, the interaction energy, with the above screening, may be as low as $\sim 10^{-4}$ eV, suggesting that strong, direct energy interactions may exist only between nearest neighbors. We note that relaxing linearization of the Poisson−Boltzmann equation (as required by $U(R) \gg kT$) would reduce the interaction energy.

**Case of a Rather Stiff Polyelectrolyte: Xanthan.** Figure 3 shows $I(q)$ for xanthan for various values of $C$ at no added salt. The peaks are much broader than the corresponding peaks for PGS in Figure 2a, so that

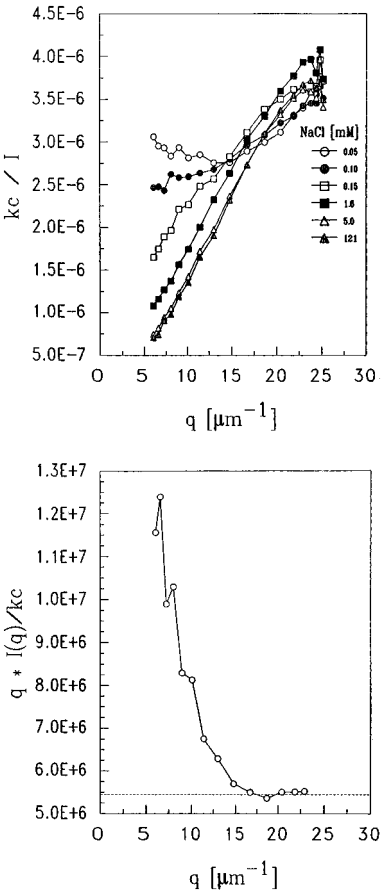


**Figure 4.** (a, top) $Kc/I(q)$ at different [NaCl] for xanthan at 0.03 mg/mL. (b, bottom) $qI(q)/Kc$ vs $q$ for xanthan at 0.03 mg/mL with [NaCl] = 12.3 mM, showing a wormlike chain nature.

the resolution of the associated $q_p$ vs $C$ for the peaks is too low to determine if the scaling is $^1/_3$ or $^1/_2$, and, in fact, attempted fits give exponents between these values. The peak of $I(q)$ for xanthan at 0.03 mg/mL falls conveniently within the mid-range of accessible $q$-values, so that this concentration was chosen for most of the experiments involving xanthan mixed with other species.

Figure 4a shows $Kc/I(q)$ of xanthan for titration with NaCl. Interestingly, the type of "still point" seen in the titration of PGS with NaCl also exists for low [NaCl]; i.e., there is a value of $I$ near $q \sim 14\ \mu m^{-1}$ which is independent of $C_s$. $P(q)$ for xanthan, used for extracting $S(q)$ from $I(q)$ subsequently, is obtained from the high-salt $I(q)$ in Figure 4a, assuming $I(q) = KcMP(q)$. As seen, there is very little change in the form of $P(q)$ after about 1 mM salt concentrations, so we take this $P(q)$ to hold down to the extremely low ionic strength limit.

Whereas xanthan is a rather stiff polyelectrolyte, we do not consider it as a rod under the conditions studied, but rather as a wormlike chain. Although there may be some discussion about whether the xanthan is in the "ordered" (high-salt) or "disordered" (low-salt) state,[29] we take $P(q)$ at high ionic strength as our operational form factor. If the xanthan is indeed disordered in the extremely low ionic strength cases where the scattering peak is observed, the molecule will be even more flexible than the following estimates suggest: Using $M = 3.6 \times 10^6$, and the mass per unit contour length $M/L = 2000$/nm from ref 29, gives a contour length, $L$, of 1800 nm. Using the wormlike chain formula for the mean square radius of gyration $\langle S^2 \rangle$ (where $R_g \equiv \langle S^2 \rangle^{1/2} = 268$ nm)

$$\langle S^2 \rangle = \frac{LL_p}{3} - L_p^2 + 2L_p^3/L - 2(L_p^4/L^2)[1 - \exp(-L/L_p)] \quad (25)$$

yields $L_p = 150$ nm, where $L_p$ is the polymer persistence length. This is in rough agreement with the value of 125 nm from ref 29. This corresponds to a number of statistical (or Kuhn) segment lengths $N \sim 6$, which indeed places the xanthan as a wormlike chain, between the rod and coil limits.

A cross-check on this can be made from Figure 4b, where a type of "Holtzer plot" is made of $qI(q)/Kc$ vs $q$ for xanthan at 0.03 mg/mL and 12.3 mM NaCl. The shape is reminiscent of a wormlike chain in which a plateau is reached at high $q$, indicative of local rodlike character on the corresponding length scale. Normally, a peak would be apparent before the plateau, but in Figure 4b, this peak is probably below the lowest observable $q$. The ratio of peak to plateau is then at least 2.2, which corresponds roughly, following the procedure of Schmidt et al.,[39] to $N_k = 10$, in reasonable agreement with the previous estimate. The value of the plateau itself, is related to $M/L$ by

$$\left.\frac{qI(q)}{Kc}\right|_{\text{plateau}} = \pi\frac{M}{L} \quad (26)$$

This yields $M/L = 1750$/nm, in fair agreement with the value of 2000/nm from ref 29.

Figure 5a shows the $I(q)/Kc$ for xanthan at 0.03 mg/mL and varying [NaCl]. Figure 5b shows the $S(q)$ found from the $I(q)$ of Figure 5a and $P(q)$ from Figure 4a. Again, a high-contrast peak is obtained for $S(q)$. Similarly to the PGS case, the peak for xanthan does not shift position as small amounts of salt are added. This again strengthens the argument that the peak corresponds to the average distance between xanthan polymers and is not measuring an electrostatic screening length. We can estimate this average interparticle spacing. At a concentration of 0.03 mg/mL, the number density, $N$, of xanthan is about 5.0 $\mu m^{-3}$. If we assume cubic packing (i.e., average interparticle distance $D_{av} \approx N^{-1/3}$), we get $D_{av} \sim 0.585\ \mu m$. If, on the other hand, we assume rodlike packing (i.e. $D_{av} \approx (LN)^{-1/2}$), and $L \approx 1.8\ \mu m$ (obtained by dividing the mass, $3.6 \times 10^6$, by the linear mass density, $2 \times 10^6/\mu m$), we get $D_{av} \sim 0.33\ \mu m$. These estimates neatly bracket the separation estimated from $D_{av} \approx 2\pi/q_p \sim 0.4\ \mu m$. That is, we are in a concentration range for which the assumption of cubic or rodlike packing does not significantly affect the estimated interparticle separation.

Following eqs 9b,c for an estimate of interaction energy range between two xanthan molecules at this concentration ($R = D_{av} \sim 585$ nm), estimating a titration charge of about 5100 for $M = 3.6 \times 10^6$, yields $U(R) \sim 32800kT$, for the bare interaction, and $10.3kT$, *using* $\kappa = 15.2\ \mu m^{-1}$ due to the counterions of the xanthan. As in the case of PGS, it is again plausible that large interaction energies exist which make neighboring molecules stay near $D_{av}$.

The $g(r)$ obtained from the $S(q)$ are shown in Figure 5c. Similar to the case of PGS, these $g(r)$ also appear to have a sort of damped quasi-periodic form. In fact, we can fit $g(r) = e^{-U(r)/kT}$, with $U(r)$ from eq 24 to our data, with $\kappa$ and $R$ as adjustable parameters, as shown in Figure 5c. In fact, the first two maxima in $g(r)$ (associated with the first two minima in $U(r)$) correspond well to $R$ and $2R$, when $R \sim 0.4\ \mu m$ by the above estimates. Interestingly, the values of $\kappa$ which optimize

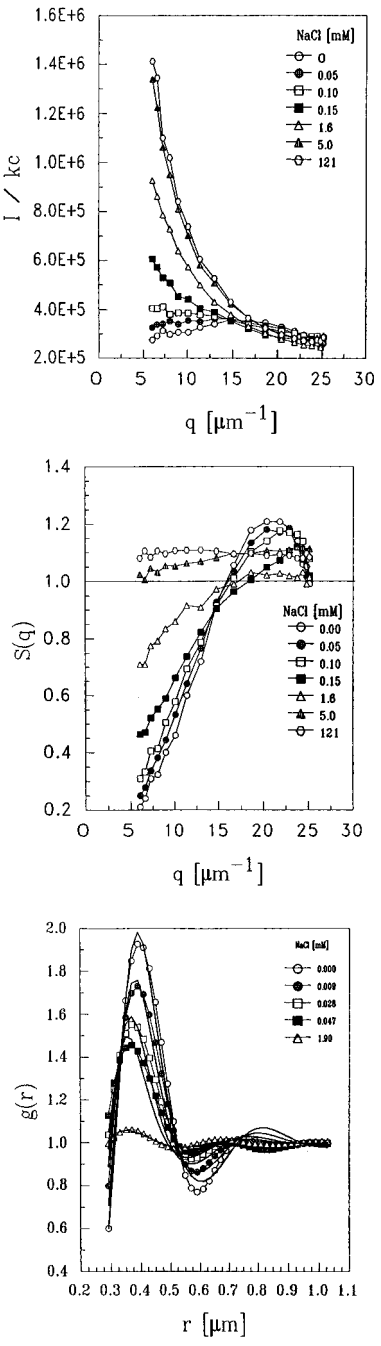


**Figure 5.** (a, top) $I(q)/Kc$ for xanthan at various $C_s$. (b, middle) $S(q)$ from the $I(q)$ of a and $P(q)$ from high-[NaCl] curves from Figure 4a. (c, bottom) $g(r)$ for xanthan from b. (See the Appendix for the details of obtaining $g(r)$ from $S(q)$.) Also shown are fits using the $U(r)$ from eq 24.

the fits give screening lengths $\kappa^{-1}$, roughly 5 times longer than those computed by

$$\kappa^2 = \kappa_0{}^2 + 8\pi l_B N_{NaCl} \tag{27}$$

where $\kappa_0$ is the screening due to the xanthan counterions and $N_{NaCl}$ is the number density of $Na^+$ or $Cl^-$ ions. This higher effective screening length found in the fits may reflect the three body (and higher) effects built into the phenomenological form for $U(r)$ in eq 24.

**Case of a Semiflexible Polyelectrolyte: Hyaluronate.** Figure 6 shows that the scattering signal, $I(q)/Kc$, from HA is basically a noise signal, scarcely above the pure water scattering level (the magnitudes of $Kc/I \sim O(10^{-4})$ are $\gg 1/M_{HA}$). Why is there no peak for HA?

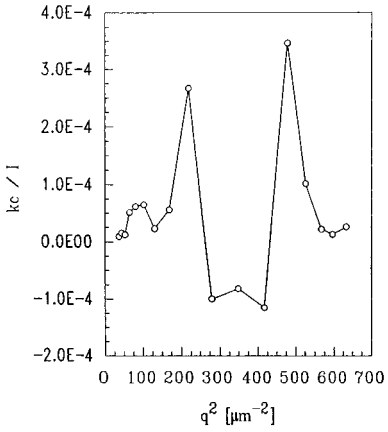


**Figure 6.** $Kc/I(q)$ vs $q^2$ for HA at 0.03 mg/mL in salt free solution. This signal is basically just noise.

We might argue that even in dilute solution the center of mass separations (CM) are not mutually exclusive for random coils, for which absolutely no symmetry exists, so that $g(0) \neq 0$ and $g(r)$ is a gradually and monotonically increasing function of $r$, leading to no strong $q$ dependence. It is pointed out that HA in all other ways exhibits the properties expected of a long, semiflexible polyelectrolyte; its root mean square radius of gyration $R_g$ and its second virial coefficient $A_2$ both strongly decrease with increasing $C_s$, and in fact the behavior of these latter two quantities vs $C_s$ is quantitatively predictable using combined electrostatic persistence length and electrostatic excluded volume theories.[32] Furthermore, the reduced viscosity $\eta_r$ vs [HA] under increasing dilution with a fixed ionic strength aqueous stock yields a peak characteristic of many polyelectrolytes.[40,41]

**II. Scattering from Mixtures of Polyelectrolytes.** The following systems of mixed polyelectrolytes were tested: (1) charged chain and small, neutral polymer, xanthan + dextran; (2) charged chain and small, same charge polyelectrolyte, xanthan + PSS; (3) charged chain and large, same sign polyelectrolyte, xanthan and HA. All the polyelectrolytes (xanthan, HA, and PSS) are polyanions.

**Charged Chain and Neutral Polymer: Xanthan and Dextran.** Figure 7a shows $I_{total}(q)/Kc$ for xanthan at 0.03 mg/mL in pure water as it is titrated with $M =$ 15 000 neutral dextran. The stock dextran solution has a concentration of 5 mg/mL, and a total of 1 mL is added to 10.15 mL of xanthan, resulting in a final dextran concentration (in the mixture) of 0.45 mg/mL and a final xanthan concentration 10% lower than its initial value. The result is that the shape of the peak is unaffected by the presence of the dextran, and the intensity increases at all $q$, the intensity at low $q$ rising somewhat faster than at high $q$; i.e. there is an increasing, slightly $q$-dependent intensity offset with increasing dextran, but no change in either the peak position or shape. Also shown in the figure is the scattering of pure dextran. The total scattering intensity, $I_{total}(q)$, adapted from eqs 17 and 18, is given by

$$I_{total}(q) = S_x(q)\, P_x(q) K_x c_x M_x + S_{xd}(q)[K_x c_x M_x K_d c_d M_d P_x(q) P_d(q)]^{1/2} + S_d(q)\, P_d(q) K_d c_d M_d \tag{28}$$

Here the x-subscripted variables are those pertinent to xanthan, and the d-subscripted variables are for dextran. $S_{xd}$ is the partial structure factor for xanthan/dextran interactions. Since d$n$/d$c$ is quite similar for

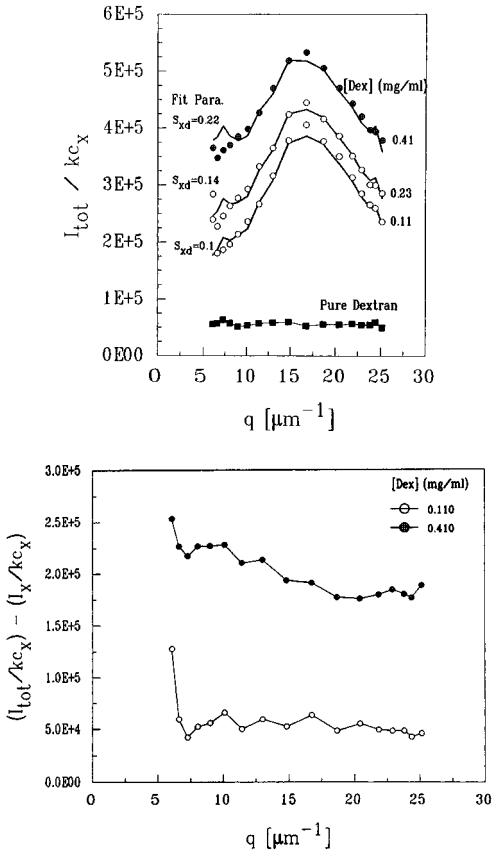


**Figure 7.** (a, top) $I_{total}(q)/Kc$ for xanthan at 0.03 mg/mL in pure water and different concentrations of dextran. Also pure dextran scattering at [dextran] = 0.41 mg/mL. Fits are to eq 29, as explained in text. (b, bottom) $I_{total}(q)/Kc$ from a with the xanthan peak at [dextran] = 0 subtracted.

dextran and xanthan, the approximation is made that $K = K_x = K_d$. It is then convenient to write the above equation as

$$I_{total}(q)/Kc_x = S_x(q)\,P_x(q)M_x + S_{xd}(q)[(c_d/c_x)M_dM_xP_x(q)P_d(q)]^{1/2} + S_d(q)\,P_d(q)(c_d/c_x)M_d \quad (29)$$

All of the factors in the above equation are known to a good approximation, except $S_{xd}(q)$, which can be taken as a constant and treated as a single adjustable parameter. The dextran is small enough that $S_d(q) \sim 1$ and $P_d(q) \sim 1$. Referring to Figure 7a with [dextran] = 0, the first term ranges from about $1.5 \times 10^5$ to $4 \times 10^5$. Over the range of added dextran, the third term ranges from 0 to $2 \times 10^5$. The square root term ranges from 0 to $8.47 \times 10^5 S_{xd}(q)$. Hence all three terms can contribute significantly to the total scattering intensity as dextran is added. The heavy solid lines in Figure 7a are fits to eq 29, using the experimental $S(q)$ for [dextran] = 0 for $S_x(q)$ and treating $S_{xd}(q)$ as an adjustable, $q$-independent constant.

It is expected that, at these concentrations, the neutral dextran has no effect on how xanthan acts with itself; hence $S_x(q)$ and $P_x(q)$ remain unaffected by the presence of dextran, so the first term likewise does not change as dextran is added. By the same argument, there is no electrostatic interaction between xanthan and dextran, so $S_{xd}(q)$ is not expected to manifest any strong correlation behavior. Fitting the curves in Figure 7a with a constant $S_{xd}(q) = S_{xd}$ yields the reasonably good fits shown. The modest change in angular dependence as dextran is added is successfully accounted for by the factor of $(P_x(q))^{1/2}$ in the cross-term, showing that $S_{xd}(q)$ is indeed constant and that the xanthan peak (first term) remains unaffected by the presence of dextran. Figure 7b shows the result of subtracting off the pure xanthan peak (first term in eq 29), showing the monotonic, angular (cross-term) function which is left. The actual interpretation of the magnitude of the fitting parameter, which is always less than unity, however, is not clear.

This behavior is qualitatively sensible: The dextran, being neutral, should have no electrostatic interaction with the xanthan. The concentrations of xanthan and dextran are so low that their steric interactions are quite negligible, so that the $g(r)$ representing dextran/xanthan interactions is flat and featureless. Hence the $g(r)$ term for xanthan/xanthan interactions is unchanged by the dextran, and the peak, given by the $I_x(q)$ term is unchanged. The cross-term is actually a "beating" term. The dextran is quite compressible and wanders freely amidst the forest of incompressible xanthan molecules, and the lack of correlation between dextran and xanthan allows the large scattered electric field from each xanthan molecule to combine with the weak scattered field from the uncorrelated dextran, giving a significant increase in net scattering; i.e $S_{xd}(q) \sim$ constant at all angles.

**Charged Chain and Same Charge Polyelectrolytes; Xanthan with PSS and Xanthan with HA.** A small ($M = 35\,000$), highly charged polyelectrolyte was next added to xanthan solutions in pure water. Adding PSS yields a shift of the peak toward higher $q$ as [PSS] increases, and some increase in scattering at $q = 0$. The effects are dramatically different than that due to adding the neutral dextran, and typical results are shown in Figure 8a. The peak shift toward higher $q$ suggests that the xanthan is actually becoming more concentrated as [PSS] increases. Parts b and c of Figure 8 show $S_x(q)$, in which the peak shift is even more striking, and $g_x(r)$, respectively.

Addition of large, highly charged HA to a 0.03 mg/mL xanthan solution in pure water led to a displacement of the xanthan peak toward higher $q$, quite similar to the case of adding the small polyelectrolyte PSS, with a concomitant increase of the $q = 0$ scattering intensity. This is shown in Figure 9a. Again, the shifting of the peak to higher $q$-values suggests that the xanthan is being concentrated by addition of the HA. Parts b and c of Figure 9 show $S_x(q)$ and $g_x(r)$, respectively.

In computing $S(q)$ and $g(r)$ for the cases of PSS and HA, we are assuming that these refer to the xanthan/xanthan contributions alone, that is, $S_x(q)$ and $g_x(r)$. This is based on the fact that the pure scattering for HA and PSS are both negligibly low, and hence the third term in eq 28 is ignored. Secondly, it is assumed that the correlations between PSS or HA and xanthan are very strong so that $S_{xd}(q) \ll 1$ over the observable $q$. Then, for PSS, $M_{PSS}$ and $c_{PSS}$ in the second term should make the second term much smaller than the first in eq 28, so that $I_{total}(q)$ essentially measures only the xanthan scattering. Since the HA behavior is quite similar to that of PSS with xanthan, we argue similarly, even though $M_{HA} \gg M_{PSS}$. Also, $c_{HA} \sim c_X$ at the highest $c_{HA}$. Finally, the $I_{total}(q)$ seen in Figures 8a and 9a is quite similar to that of the pure xanthan of Figure 3, suggesting that the scattering is indeed coming essentially from the xanthan, without the second and third terms of eq 28 changing the aspect of $I_{total}(q)$.

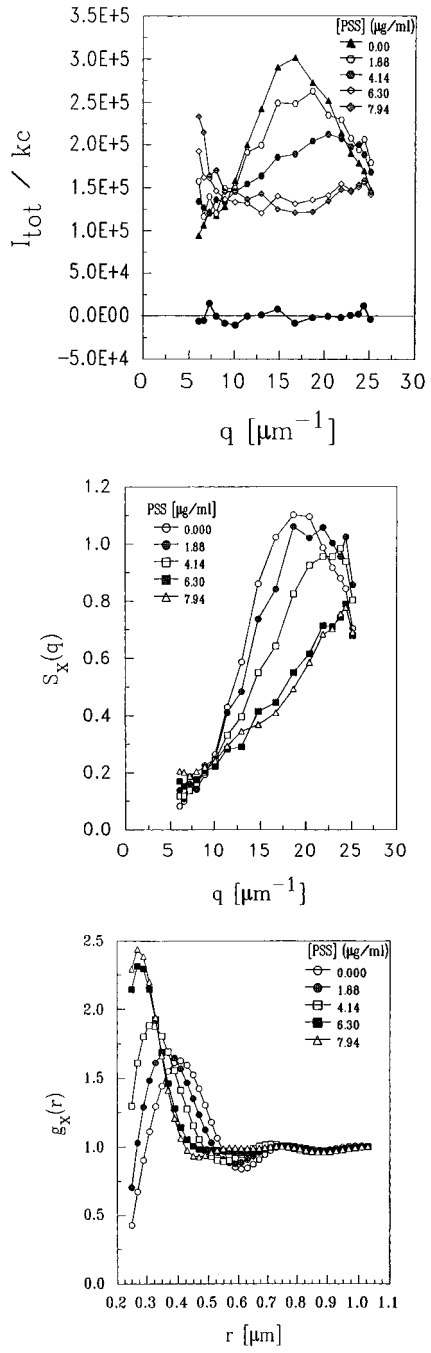


**Figure 8.** (a, top) $I_{total}(q)/Kc$ for 0.03 mg/mL xanthan in pure water and different concentrations of PSS. Also shown is pure PSS at 0.008 mg/mL in water. (b, middle) $S_x(q)$ from a and the $P(q)$ from the high-[NaCl] curves in Figure 4a. (c, bottom) $g_x(r)$ from b.

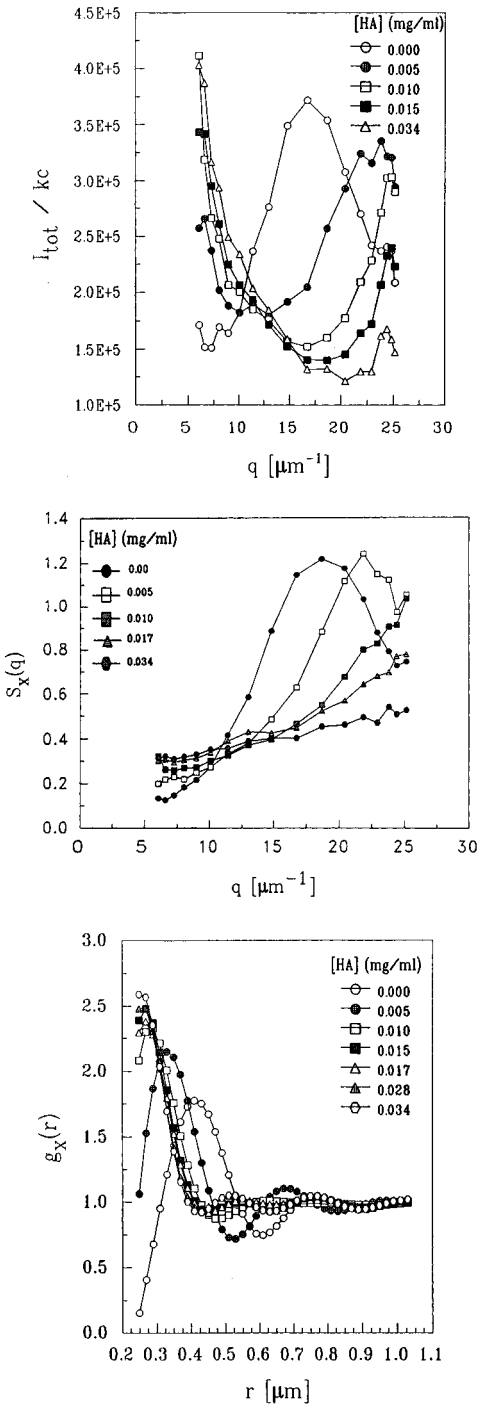


**Figure 9.** (a, top) $I_{total}(q)/Kc$ for 0.03 mg/mL xanthan in pure water and different concentrations of HA. (b, middle) $S_x(q)$ from a and $P(q)$ determined from the high-[NaCl] curves of Figure 4a. (c, bottom) $g_x(r)$ from b.

The main feature of adding both PSS and HA to xanthan solutions is the peak shift toward higher $q$-values, corresponding to the notion of smaller average distance between xanthan molecules. In fact, if Figure 8a (xanthan/PSS) and Figure 9a (xanthan/HA) are compared to Figure 3 (pure xanthan peaks), the trends are strikingly similar, in terms of the peak shifting to higher $q$-values, the lowering of the peak intensity, and the absolute $I/Kc$ values involved.

The only immediate alternative to the xanthan molecules becoming more concentrated by addition of HA or PSS is if somehow the PSS or HA molecules acquire scattering properties nearly identical to those of xanthan. In that case, the whole effect could be simply interpreted as the net increase of concentration of total polymer molecules. Since HA and PSS by themselves in water scatter quite differently from xanthan (Figures 6 and 8a), however, it is not easy to accept the notion that they suddenly begin to scatter like xanthan molecules when introduced into a xanthan solution. In fact, HA and PSS by themselves at the concentrations studied scatter so feebly that they are below the limits of detection. Even if the cross-term in eq 29 became comparable to the leading term, the peak position of the leading term would not change and the cross-term would add some type of $q$-dependent term, which should not add up to the pure peak shift observed.

Hence, the most probable explanation is that addition of PSS or HA forces the xanthan molecules to a closer

average spacing, leading to the peak shift toward higher $q$. A conceptual model for this is needed, and we do not intend here to develop a rigorous explanation. Rather, we reason as follows: Pure, stochastic mixing of xanthan and HA or PSS cannot change the average inter-xanthan spacing, so such mixing is excluded. Extremely local effects of HA or PSS forcing two xanthan molecules at a time closer together also cannot work, since, for each pair of xanthans pushed closer together, there would be a pair of xanthans farther apart, which would simply lead to a broadening of the peak, not a shift in the peak. Therefore, there must be groups of xanthan molecules which are forced locally together, in sufficient number that the effect of the interparticle scattering within the groups dominates the total scattering (correspondingly HA or PSS are also forced into similar groups, which scatter no detectable light). *A priori*, we have no idea of how many xanthans are involved in such groups. The extreme case, of course, would be the total phase separation of the xanthan from the PSS or HA. While complete phase separation would be sufficient to account fully for the data, it is not necessary to explain it. Although we do not exclude the possibility of complete phase separation, it does not seem likely to happen at the extremely low concentrations of polyelectrolytes being studied. It is possible that at these low concentrations the xanthan groups formed are actually the result of dynamic fluctuations which are weighted toward the formation of transient xanthan groups. The thermodynamic weighting which would lead to such groups would come ultimately from the net free energy difference between pure, stochastic mixing and the dynamic groups. While this notion should furnish considerable grist for theoretical computations, we do not address it here. Rather, we will confine ourselves to estimating, from our scattering data, the minimum size of these xanthan enhanced regions.

These regions of increased xanthan concentration (accompanied, obviously, by xanthan poor regions) will themselves scatter light, over and above that scattered by the xanthan molecules themselves. Their size is constrained by the fact that we see little evidence of this scattering; i.e. in the extreme case of complete phase separation there would be no low-$q$ scattering, but for some minimum size of the xanthan rich regions a detectable low-$q$ scattering would be expected. For a rough estimate, we assume this scattering will vary as

$$I_G/Kc_G = M_G P(q) \tag{30}$$

where the subscript G refers to the xanthan rich polymer groups, and all physical parameters are those for the xanthan groups. Clearly, the mass concentration, $c_G$, is the same as that for xanthan itself, $c_X$. If, as we assume, the refractive index increment, $\partial n/\partial c$, is the same for the groups as for the xanthan itself when uniformly distributed, then the left side of eq 30 can be compared directly with Figure 7a and Figure 8a. The mass of such a xanthan-rich group, assumed to be roughly spherical, is given by

$$M_G \approx c_X' N_{AV} \frac{D^3}{2} = r c_X N_{AV} \frac{D^3}{2} \tag{31}$$

where $D$ is the diameter of the sphere, and $c_X' = rc_X$ is the enhanced concentration of xanthan. For spherical groups, we can use the standard form factor, eq 4. The first root of this form factor occurs at $x \approx 4.5$, or $q \approx 9/D$, where $x = qD/2$. Inspection of our data shows no scattering from such xanthan groups at the lowest measurable $q$ value (except possibly the scattering that arises at very low $q$ as polyelectrolyte is added), which implies the value of $q$ above must be less than about 6 $\mu m^{-1}$, giving a diameter no less than about 1.5 $\mu$m. Since the peak in $S(q)$ shifts from $q_p \sim 18\ \mu m^{-1}$ to at least 25 $\mu m^{-1}$, we know the concentration enhancement factor is roughly $r \approx (25/18)^3 \sim 2.5$. With this, we can estimate the *minimum* mass of the xanthan groups from eq 31 as $M_G \approx 8 \times 10^7$ g·mol$^{-1}$, which is roughly consistent with about 30 xanthan molecules, each occupying a volume of $\sim 4R_g^3$, packed in a sphere of diameter 1.5 $\mu$m.

## Summary

The static light scattering peaks for highly charged polyelectrolytes at extremely low ionic strength and polyelectrolyte concentration have been studied for pure polyelectrolytes and various mixtures. For the case of the pure polyelectrolytes, xanthan and proteoglycan subunit, the experimental $P(q)$ has been used to extract the structure factor $S(q)$, which displays a high-contrast peak. Hence, none of the $S(q)$ predicted from such models as the correlation hole ($S(q)$ monotonically increasing), the electrostatically enhanced square well potential (low-contrast $S(q)$ peak), or the point charge/point charge interaction ($S(q) \propto q^2/(\kappa^2 + q^2)$) correctly describes the experimental $S(q)$ for these experimental conditions. Computing the transforms of $S(q)$ to yield the pair correlation function $g(r)$ suggests that the scattering peaks are due to dynamic correlations between neighboring particles via a rapidly damped quasi-periodic screened potential. The peak of the scattering curve $I(q)$ occurs at a value of $q$ which clearly measures the interparticle spacing, not any type of electrostatic screening or other scaling length. In this picture, the particles diffuse about quite rapidly; that is, there is no long-range order or liquid crystalline structure, and they fluctuate fairly narrowly about a nearest neighbor distance corresponding to the average interparticle spacing. There is no slow mode of diffusion associated with the existence of the static scattering peak which would suggest any type of clustering or ordered structures.

Addition of neutral polymer to xanthan causes no peak shift, indicating that the dextran/xanthan interaction is negligible. The cross-term in the intensity in this case provides a significant, weakly $q$-dependent increase in the scattering. When large (HA) or small (PSS) polyelectrolytes are added to the xanthan, however, the peak undergoes a shift to higher $q$ values, suggesting increased xanthan concentration. Because of the high correlation between PSS or HA and xanthan, the cross-term in eq 28 does not contribute significantly, in contrast to the neutral dextran case. The tentative interpretation of the result for these mixtures is that the repulsive interactions between xanthan and PSS or HA are greater than those between xanthan/xanthan and PSS/PSS or HA/HA, leading to local concentration fluctuations in which groups of xanthan molecules are forced closer together.

**Acknowledgment.** We gratefully acknowledge support from the National Science Foundation for Grants MCB-99116605 and the Center for Photoinduced Processes, which is also funded in part by the Louisiana Board of Regents. M.B. acknowledges the Fulbright Commission for support during his stay at Tulane University.

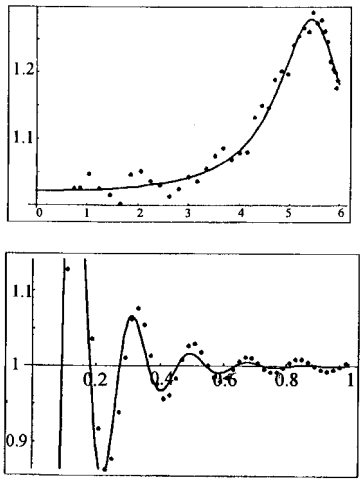


**Figure 10.** (a, top) Hypothetical, analytic $S(q)$ vs $q$ (solid line) with simulated "data" as filled circles. Note the addition of random noise (±5%) to the sampled points. (b, bottom) Analytic transform of $S(q)$ from a vs $r$ (solid line) with numerical transform of sampled points (filled circles). Note the expanded scale to better indicate the deviation (on full scale, the deviation is difficult to discern).

## Appendix: Considerations on the Fourier Transform of $S(q)$ to Obtain $g(r)$

It is well-known that the pair distribution function and the structure factor are related by a Fourier transform, and, upon averaging over all possible orientations of the scattering molecules, this transform takes the form (from eq 21)

$$g(r) = 1 + \left(\frac{1}{2\pi^2 N}\right)\left(\frac{1}{r}\right)\int_0^{+\infty} q[S(q) - 1]\sin(qr)\,\mathrm{d}q \quad \text{(A1)}$$

Thus, given the structure factor, $S(q)$, it is, in principle, straightforward to obtain the pair distribution function, $g(r)$. In practice, however, there are difficulties. Experimentally, one never obtains $S(q)$ for all possible values of $q$. Rather, one obtains $S(q)$ over a limited range of $q$ and only for discrete values of $q$ in that range. We consider the latter point first.

Discrete, as opposed to continuous, sampling of the structure factor raises the concern of aliasing when reconstructing $g(r)$. That is, when measuring $S(q)$ at discrete, separated points, one risks missing structure in $S(q)$ that occurs between the sampled points. This structure would correspond to values of $g(r)$ at large $r$; the more closely spaced the sampling, the larger the value of $r$. One is then led to consider the sampling theorem,[42] which states that a function is fully specified by values taken at intervals of $\Delta q$, so long as the Fourier transform of the function is zero for values of $r > \pi/\Delta q$. So, sampling $S(q)$ at intervals $\Delta q \sim 1\ \mu\mathrm{m}^{-1}$ ($\Delta q \sim 0.43\ \mu\mathrm{m}^{-1}$ for proteoglycan data) is sufficient if $g(r)$ is one for $r > 3\ \mu$m ($r > 7.2\ \mu$m for proteoglycan data). In our experiments, we estimate the counterion charge density for xanthan at 0.03 mg/mL as $N_{ci} \sim 2.5 \times 10^{16}\ \mathrm{cm}^{-3}$, which gives a screening length of $\kappa^{-1} \sim 0.07\ \mu$m. For the proteoglycans at 0.253 mg/mL, we estimate the counterion charge density as $N_{ci} \sim 2.8 \times 10^{17}\ \mathrm{cm}^{-3}$, which gives a screening length of $\kappa^{-1} \sim 0.02\ \mu$m. Given such short screening lengths, it is extremely unlikely that any particle correlations exist at such a large distance. Using a simple screened Coulomb potential, we estimate the interaction energy at this large distance as $\sim 10^{-20}$ eV, that is, effectively zero. It is sufficient, then, to describe $g(r)$ by a discrete sum (i.e. a Fourier sine series), rather than a Fourier sine transform. That finite sum is given by

$$g(r_j) = 1 + \left(\frac{1}{2\pi^2 N}\right)\left(\frac{1}{r_j}\right)\sum_i q_i[S(q_i) - 1]\sin(q_i r_j)\Delta q_i \quad \text{(A2)}$$

Consider now the finite range over which $S(q)$ is measured.

The concern now is whether we have a sufficient range on $q$ to ensure the convergence of the series given in eq A2. To investigate this, we carried out an extensive series of simulated experiments. That is, we postulated a hypothetical pair distribution function, $g(r)$, for which we could analytically determine the structure factor, $S(q)$, and whose structure factor is qualitatively similar to our data. We then sampled this $S(q)$ just as in our experiments. We then subjected this "data" to the transform A2 and compared the resultant "experimental" $g(r)$ to the original. Additionally, we investigated the effects of adding random and systematic errors to the simulated data. A typical result is shown in Figure 10. Figure 10a shows the analytical $S(q)$ (as a solid line) along with the sampled points, and Figure 10b shows the original $g(r)$ (again, a solid line) along with the distribution function obtained from the transform A2. The results are impressive, particularly when considering that no windowing was performed on the data prior to applying the transform A2. However, we stress that, in the interests of conservatism, we applied a Parzen, or triangular, window (i.e. zero at high and low $q$-values and 1 at the mid-range q-value) to all experimental data before applying the transform A2. The Parzen window, like most windowing methods, suppresses spurious oscillations in transformed data at the cost of some small amount of broadening of the structure revealed by the transform. In brief, the conclusions drawn from the simulated experiments are (A) that the $g(r)$ obtained from the transform A2 converges well to the postulated $g(r)$ so long as the amplitude of the error (whether random or systematic) is small compared to the amplitude of the structure factor; that is, $\delta S \ll (S_{max} - S_{min})$ and (B) that the structure factor have high contrast ($2[S_{max} - S_{min}] \sim [S_{max} + S_{min}]$); if it is not (i.e. if $S_{max} - S_{min} \ll 1$), the $g(r)$ obtained is dominated by spurious structure. Both conditions are satisfied by our data.

## References and Notes

(1) Nierlich, M.; Boue, F.; Lapp, A.; Oberthur, R. *J. Phys. (Paris)* **1983**, *44*, 87. Nierlich, M.; Williams, C. E.; Boue, F.; Cotton, J. P.; Daoud, M.; Farnoux, B.; Jannink, G.; Picot, C.; Moan, M.; Wolff, C.; Rinaudo, M.; de Gennes, P. G. *J. Phys. (Paris)* **1979**, *40*, 701.
(2) Nallet, F.; Jannink, G.; Hayter, J.; Oberthur, R.; Picot, C. *J. Phys. (Paris)* **1983**, *44*, 87.
(3) de Gennes, P. G. *Scaling Concepts in Polymer Physics*; Cornell University Press: Ithaca, NY, 1979.
(4) Wang, L.; Bloomfield, V. A. *Macromolecules* **1991**, *24*, 5791.
(5) Maier, E. G.; Krause, R.; Deggelmann, M.; Hanegbuchle, M.; Weber, R.; Fraden, S. *Macromolecules* **1992**, *25*, 1125.
(6) Drifford, M.; Dalbiez, J. P. *J. Phys. Chem.* **1984**, *88*, 5368.
(7) Li, X.; Reed, W. F. *J. Chem. Phys.* **1991**, *94*, 4568.
(8) Forster, S.; Schmidt, M.; Antonietti, M. *Polymer* **1990**, *31*, 781.
(9) Morfin, I.; Reed, W.; Rinaudo, M.; Borsali, R. *J. Phys. (Paris)* **1994**, *4*, 1001.
(10) Genz, U.; Klein, R.; Benmouna, M. *J. Phys. (Paris)* **1989**, *50*, 449.
(11) Sedlak, M.; Amis, E. J. *J. Chem. Phys.* **1992**, *96*, 826.
(12) Ghosh, S.; Peitzsch, R. M.; Reed, W. F. *Biopolymers* **1992**, *32*, 1105.

(13) Peitzsch, R. M.; Burt, M. J.; Reed, W. F. *Macromolecules* **1992**, *25*, 806.
(14) Smits, R. G.; Kuil, M. E.; Mandel, M. *Macromolecules* **1994**, *27*, 5599.
(15) Yamakawa, H. *Modern Theory of Polymer Solutions*; Harper and Row: New York, 1971.
(16) Higgins, J. S.; Benoit, H. *Polymers and Neutron Scattering*; Oxford Science Publications: Oxford, U.K., 1994.
(17) Hansen, J. P.; McDonald, I. R. *The Theory of Simple Liquids*; Academic Press: New York, 1986.
(18) March, M.; Tosi, M. In *Atomic Dynamics in Liquids*; Landau, Ed.; Macmillan: New York, 1976.
(19) Hayter, J. B.; Penfold, J. *Mol. Phys.* **1981**, *42*, 109.
(20) Belloni, L. Ph.D. dissertation, University Pierre and Marie Curie, Paris VI, 1982.
(21) Dolar, D. In *Polyelectrolytes, Charged and Reactive Polymers*; Selegny, E., Mandel, M., Strauss, U. P., Eds.; Reidel: Dordrecht, The Netherlands, 1974; Vol. 1.
(22) van der Maarel, J. R. C.; Groot, L. C. A.; Mandel, M.; Jesse, W.; Jannink, G.; Rodriguez, V. *J. Phys. II* **1992**, *2*, 109.
(23) van der Maarel, J. R. C.; Groot, L. C. A.; Hollander, J. G.; Jesse, W.; Kuil, M. E.; Leyte, J. C.; Leyte-Zuiderweg; Mandel, M.; Cotton, J. P.; Jannink, G.; Lapp, A.; Farago, B. *Macromolecules* **1993**, *26*, 7295.
(24) Grimson, M.; Benmouna, M.; Benoit, H. *J. Chem. Soc., Faraday Trans.* **1988**, *85*, 1563.
(25) Benmouna, M.; Vilgis, T.; Hakem, F.; Negadi, A. *Macromolecules* **1991**, *24*, 6418.
(26) Wyatt, P. *Anal. Chim. Acta* **1993**, *272*, 1.
(27) Morris, E. R.; Rees, D. A.; Young, G.; Walkinshaw, M. D.; Darke, A. *J. Mol. Biol.* **1977**, *110*, 1.
(28) Milas, M.; Rinaudo, M. *Carbohydr. Res.* **1986**, *158*, 191.
(29) Milas, M.; Reed, W. F.; Printz, S. *Int. J. of Biol. Macromol.*, in press.
(30) Paradossi, G.; Brant, P. A. *Macromolecules* **1982**, *15*, 874.
(31) Reed, W. F.; Ghosh, S.; Medjhadi, G.; François, J. *Macromolecules* **1991**, *24*, 6189.
(32) Ghosh, S.; Li, X.; Reed, C. E.; Reed, W. F. *Biopolymers* **1990**, *30*, 1101.
(33) Hardingham, T. E.; Muir, H. *Biochem. Biophys. Acta* **1972**, *279*, 401.
(34) Plaas, A. H. K.; Sandy, J. D.; Muir, H. *Biochem. J.* **1983**, *214*, 855.
(35) Heinegard, D.; Paulsson, M. In *Extracellular Matrix Biochemistry*, Piez, K. A., Reddi, A. H., Eds.; Elsevier: New York, 1984; pp 277−328.
(36) Joanny, J. F.; Leibler, L. *J. Phys. (Paris)* **1990**, *51*, 545.
(37) Benmouna, M.; Weill, G.; Benoit, H.; Akcasu, Z. *J. Phys. (Paris)* **1982**, *43*, 1679.
(38) Reed, W. F. *J. Chem. Phys.* **1995**, *100*, 7825.
(39) Schmidt, M.; Paradossi, G.; Burchard, W. *Makromol. Chem., Rapid Commun.* **1985**, *6*, 767.
(40) Rinaudo, M.; Milas, M.; Jouon, M.; Borsali, R. *Polymer* **1993**, *34*, 3710.
(41) Reed, W. F. *J. Chem. Phys.* **1994**, *101*, 2515.
(42) See, for example: Bracewell, R. D. *The Fourier Transform and Its Applications*, 2nd ed., revised; McGraw-Hill: New York, 1986; pp 189−194.

MA960148W